# Stable Quantum Dot Photoelectrolysis Cell for Unassisted Visible Light Solar Water Splitting

**Hong Bin Yang,[†] Jianwei Miao,[†] Sung-Fu Hung,[†,‡] Fengwei Huo,[§] Hao Ming Chen,[*,‡] and Bin Liu[*,†]**

[†]School of Chemical and Biomedical Engineering, Nanyang Technological University, 62 Nanyang Drive, Singapore 637459, Singapore, [‡]Department of Chemistry, National Taiwan University, No. 1, Sec. 4, Roosevelt Road, Taipei 10617, Taiwan, and [§]School of Materials Science and Engineering, Nanyang Technological University, 50 Nanyang Avenue, Singapore 639798, Singapore

**ABSTRACT** Sunlight is an ideal source of energy, and converting sunlight into chemical fuels, mimicking what nature does, has attracted significant attention in the past decade. In terms of solar energy conversion into chemical fuels, solar water splitting for hydrogen production is one of the most attractive renewable energy technologies, and this achievement would satisfy our increasing demand for carbon-neutral sustainable energy. Here, we report corrosion-resistant, nanocomposite photoelectrodes for spontaneous overall solar water splitting, consisting of a CdS quantum dot (QD) modified $TiO_2$ photoanode and a CdSe QD modified NiO photocathode, where cadmium chalcogenide QDs are protected by a ZnS passivation layer and gas evolution cocatalysts. The optimized device exhibited a maximum efficiency of 0.17%, comparable to that of natural photosynthesis with excellent photostability under visible light illumination. Our device shows spontaneous overall water splitting in a nonsacrificial environment under visible light illumination ($\lambda > 400$ nm) through mimicking nature's "Z-scheme" process. The results here also provide a conceptual layout to improve the efficiency of solar-to-fuel conversion, which is solely based on facile, scalable solution-phase techniques.

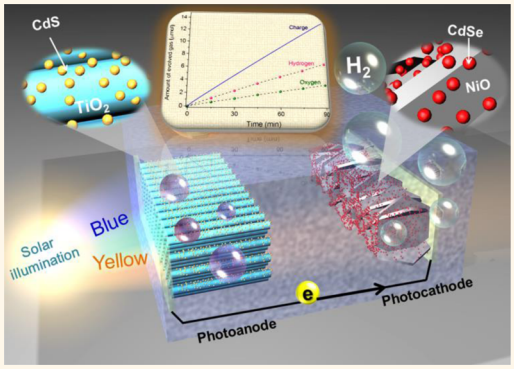


**KEYWORDS:** water splitting · quantum dots · semiconductor · photoelectrochemical cell

Sunlight is an inexpensive, nonpolluting, abundant renewable source of energy. The amount of sunlight striking Earth for a given time period is approximately 10 thousand times greater than the total energy consumed on the planet.[1,2] Thus, converting solar energy into an easily usable form has attracted substantial attention in past decades.[3] As society has become increasingly conscious of the adverse impacts of anthropogenic activities on the environment, the development of methods to efficiently harness solar energy has emerged as one of the central scientific challenges in the 21st century.[4,5] Photosynthesis in plants underpins the existence of many life-forms on Earth,[6] where a remarkable chemical reaction lies at the core of photosynthesis: the solar energy conversion of water and carbon dioxide into oxygen and carbohydrates (fuel). The development of an artificial version of this reaction, based on splitting water into oxygen and hydrogen, is highly desirable, owing to the attraction of hydrogen as a fuel.[5,7] The efficient conversion of sunlight into fuels through the photochemical splitting of water to generate hydrogen and oxygen is a critical factor for developing sustainable energy. Since Fujishima and Honda reported the first photoelectrochemical device for solar water splitting in 1972,[8] numerous research efforts have been devoted toward the development of efficient photocatalytic systems for hydrogen production.[9,10] Among them, two photocatalytic systems, namely, the single-photon system[11−13] and two-photon system, have been extensively studied.[14−17] As compared to the single-photon system, the two-photon system allows capture of lower energy photons and thus a larger part of the solar spectrum, which can potentially lead to a higher solar-to-fuel conversion efficiency. Furthermore, the reduction and oxidation catalytic centers in the two-photon system are spatially

* Address correspondence to haomingchen@ntu.edu.tw; liubin@ntu.edu.sg.

Received for review July 9, 2014 and accepted September 30, 2014.

**Published online September 30, 2014**
**10.1021/nn503751s**

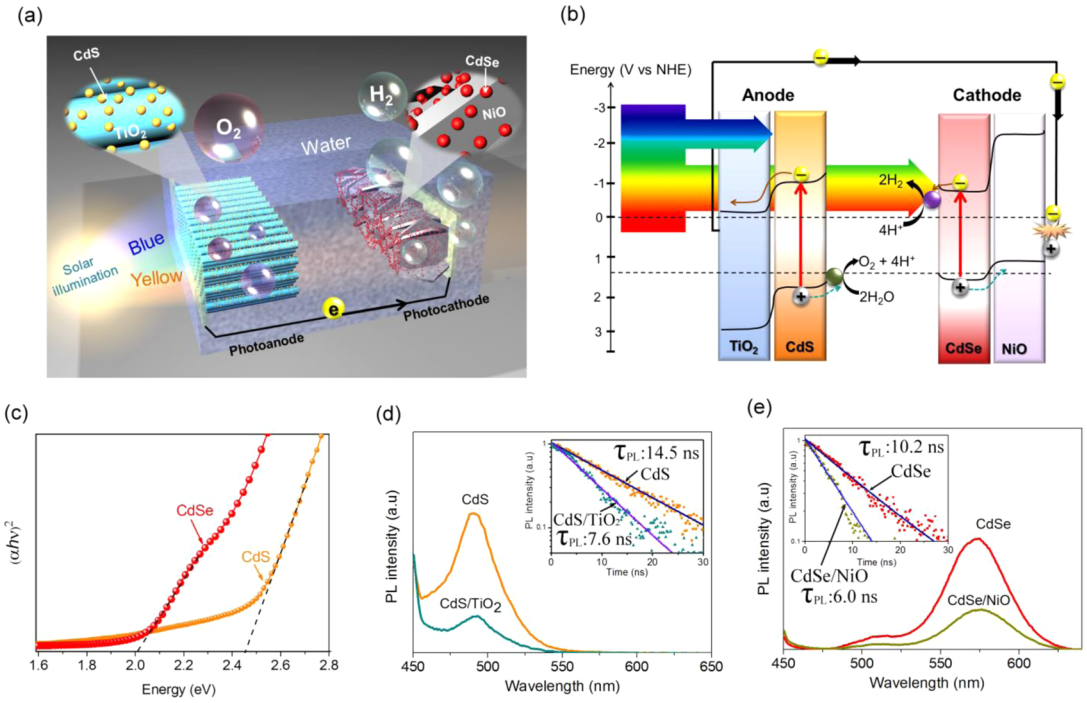


**Figure 1. (a) Cadmium chalcogenide QD modified photoelectrolysis cell system constructed with an array of CdS QD modified $TiO_2$ nanorods serving as the photoanode and CdSe QD modified NiO nanosheets serving as the photocathode. (b) Energy band diagram of a cadmium chalcogenide QD modified photoelectrolysis cell system for direct solar-driven water splitting. The photogenerated holes in the CdS QD modified $TiO_2$ nanorod photoanode and electrons in the CdSe QD modified NiO nanosheet photocathode move to the quantum dot surface to perform water splitting, while the electrons in $TiO_2$ and holes in NiO recombine at the external circuit. (c) Tauc plot of CdS and CdSe QDs. (d and e) Photoluminescence emission spectra of CdS QDs, CdS QDs adsorbed on $TiO_2$ nanorods, CdSe QDs, and CdSe QDs adsorbed on NiO nanosheets. Insets in d and e are time-resolved photoluminescence decays of CdS QDs and CdS QDs adsorbed on $TiO_2$ nanorods and CdSe QDs and CdSe QDs adsorbed on a NiO nanosheet.**

separated, which not only minimizes the undesirable back-reaction but also separates the photosynthetic products. Regarding this two-photon system, a "Z-scheme" in artificial photosynthesis would be considered for solar water splitting,[18−21] in which the photogenerated minority carriers in two semiconductors move toward the semiconductor−electrolyte interface to carry out individual half reactions while the majority carriers recombine at the ohmic contact between the semiconductors.[22] Consequently, both photoreduction reaction and water oxidation reaction can spontaneously occur in corresponding inorganic semiconductors to evolve hydrogen and oxygen, respectively.

Although unassisted solar water splitting has been achieved in previous studies of photoelectrochemical systems, some wide-band-gap semiconductors (*e.g.*, $TiO_2$) had to be employed to capture sunlight,[23,24] which only allows harvesting UV light in the solar spectrum and greatly limits their overall solar-to-fuel conversion efficiency. Regarding this issue, several strategies have been revealed to achieve the utilization of visible photons in sunlight.[25] Among which, inorganic quantum dot (QD) sensitization has been demonstrated as an effective way to extend the photoresponse of wide-band-gap semiconductors to visible light,[26,27] because of the tunable band gap by controlling the QD's size and composition. However, it is worth pointing out that their photostability and long-term durability have to be considerably addressed for future applications since the photosystem needs to be operated under tough conditions and long-term illumination. Here, we develop a cadmium chalcogenide QD modified photoelectrochemical system consisting of a CdS QD modified $TiO_2$ nanorod photoanode and a CdSe QD modified NiO nanosheet photocathode for spontaneous overall solar water splitting to produce $H_2$ and $O_2$ under visible light illumination, in which corresponding cocatalysts and surface protection were developed to considerably facilitate the stability of the system. This development is a remarkable step toward the demonstration of a complete QD-based artificial photosynthetic system that is efficient, durable, and cost-effective.

## RESULTS AND DISCUSSION

**Characterization of Photoelectrodes.** The photoelectrochemical system, which uses cadmium chalcogenide QDs as light absorbers, is depicted in Figure 1a. $TiO_2$ nanorods grown on transparent conductive fluorine-doped tin oxide (FTO) substrate decorated with CdS QDs served as an $O_2$-generating photoanode, while the photocathode for hydrogen evolution consisted of a

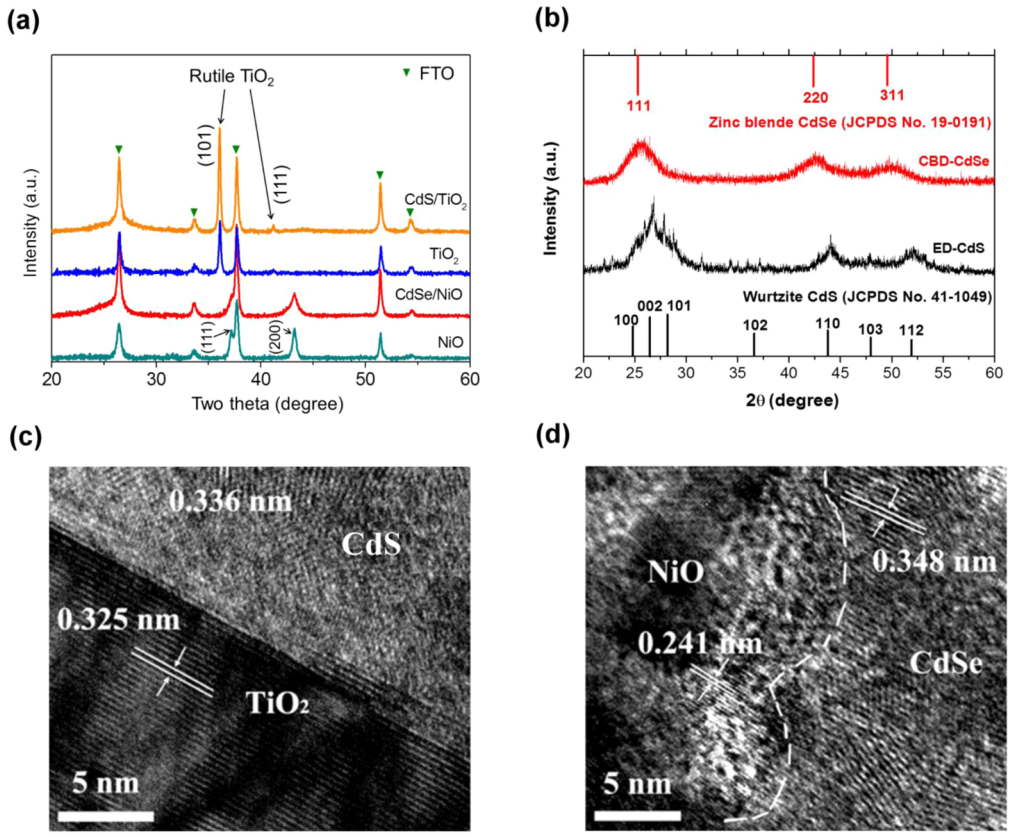


**Figure 2. (a) XRD patterns of NiO nanosheet array, CdSe QDs-modified NiO nanosheet array, $TiO_2$ nanorod array, and CdS QDs-modified $TiO_2$ nanorod array. (b) XRD patterns of CdSe (chemical bath deposition) QDs (CBD-CdSe) and CdS (electrodeposition) QDs (ED-CdS) prepared under the same conditions. (c) High-resolution TEM images of CdS QD modified $TiO_2$ nanorods. (d) High-resolution TEM images of CdSe QD modified NiO nanosheets.**

NiO nanosheet array with modification of CdSe QDs. An energy diagram of theh present CdS and CdSe QD modified $TiO_2$ and NiO photoelectrodes is plotted in Figure 1b, and the band gaps of CdS and CdSe QDs are estimated to be ~2.46 and 2.0 eV, respectively, which are larger than their bulk values due to the quantum confinement effect (Figure 1c). NiO is a wide-band-gap (~3.6 eV) p-type semiconductor, widely used as an electron-blocking and hole-transporting layer in polymer and dye-sensitized solar cells.[28−31] The frequently cited Fermi level of undoped NiO is about 5.0 eV, while the valence band maximum (VBM) is 0.4 eV below the Fermi level.[32−35] CdSe can form a type II heterojunction upon NiO with band offsets of −2.4 eV (vacuum level: −4.2 eV/−1.8 eV) and +0.8 eV (vacuum level: −6.2 eV/−5.4 eV) at the conduction and valence band, respectively. Because of the type II band alignment, photoexcited carriers in CdSe can effectively dissociate at the CdSe/NiO interface.[36] Furthermore, the conduction band of CdSe is more negative (0.3 eV) than the redox potential of $H^+/H_2$, making photocatalytic $H_2$ evolution thermodynamically favorable. In the case of the photoanode, $TiO_2$ (rutile) is a wide-band-gap (~3.0 eV) n-type semiconductor, able to form a type II heterojunction with CdS as well.[16] Upon exposure to visible light, the photoexcited carriers generated in CdS and CdSe would diffuse to CdS/$TiO_2$ and CdSe/NiO interfaces and dissociate into free electrons and holes. The photogenerated holes in CdS migrate to the CdS/electrolyte interface and oxidize water to generate $O_2$. Meanwhile, the photogenerated electrons in CdSe reduce protons to evolve $H_2$. In this design, the injection of sensitized electrons and holes from adsorbed CdS and CdSe QDs into $TiO_2$ and NiO can be revealed by time-resolved photoluminescence spectroscopy measurements. As shown in Figure 1d and e, the photoluminescence intensities of CdS and CdSe QDs were quenched by 75% and 65% once they were attached to $TiO_2$ and NiO photoelectrodes, respectively. Accompanying the formation of CdS/$TiO_2$ and CdSe/NiO junctions, a significant decrease in photoluminescence lifetime from 14.5 and 10.2 ns to 7.6 and 6.0 ns can be attributed to effective charge-carrier transferring through junctions.

In a typical procedure of QD-modified photoelectrodes, a NiO nanosheet array and CdSe QDs were grown on an FTO substrate in sequential order using a modified chemical bath deposition (CBD) method.[37,38] Notably, a 100 nm thick NiO compact layer (Figure S1) has to be prepared on the FTO surface prior to the CBD growth of NiO nanosheets, since the compact layer is

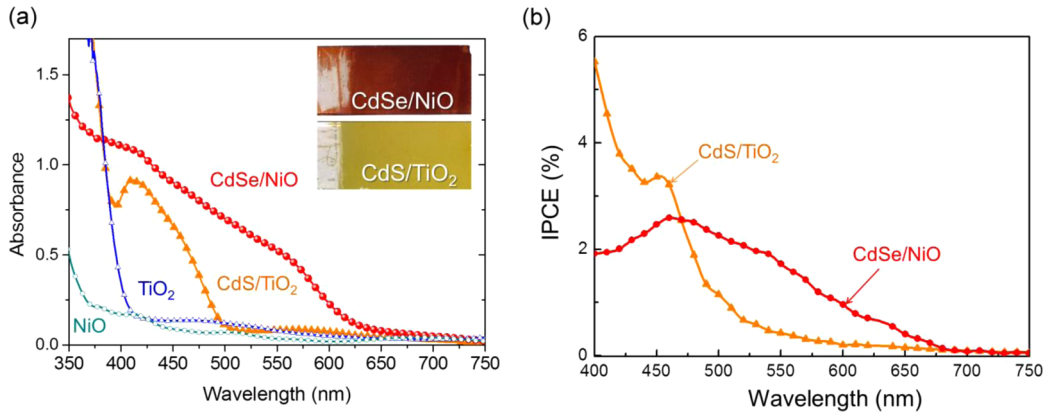


**Figure 3. (a) UV/vis spectra and photographs of CdS QD modified $TiO_2$ photoanode and CdSe QD modified NiO photocathode. (b) IPCE spectra of CdS QD modified $TiO_2$ photoanode and CdSe QD modified NiO photocathode measured at −0.3 V *vs* Ag/AgCl.**

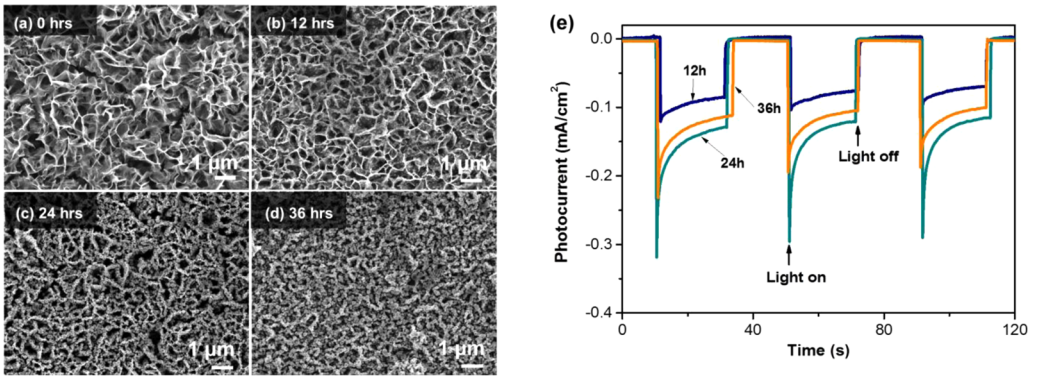


**Figure 4. SEM images of (a) NiO nanosheet array and (b−d) CdSe QD modified NiO nanosheet array with various CBD growth timesof CdSe (b, 12 h; c, 24 h; and d, 36 h). (e) Transient photocurrent response curves of CdSe-modified NiO photocathode prepared with various CdSe deposition times at 0 V *vs* Ag/AgCl.**

able to avoid a direct contact between CdSe and the FTO electrode. A control experiment shows a considerably anodic response in the CdSe/NiO nanosheet photoelectrode without a NiO compact layer owing to the direct electron injection from CdSe QDs to FTO (Figure S2).

The deposition of CdSe and CdS QDs on NiO and $TiO_2$ photoelectrodes was studied with X-ray diffraction (XRD), as shown in Figure 2a. The diffraction patterns of QD modification on the surface of $TiO_2$ or NiO were absent of obvious diffraction contribution from QDs, which can be attributed to the characteristics of the nanocrystalline nature of QDs. As a result, CdSe and CdS QDs were prepared under identical conditions to further verify their structures (Figure 2b). Several feature diffraction peaks at ~25.0° and 26.5° in the XRD patterns could be assigned to the (111) diffraction of zinc blende CdSe (JCPDS No. 19-0191) and the (002) diffraction of wurtzite CdS (JCPDS No. 41-1049), respectively. High-resolution scanning and transmission electron microscope images reveal a close contact between CdS (CdSe) QDs and $TiO_2$ nanorods (NiO nanosheets) (Figure 2c and d and Figure S3). Notably, apparent contrasts between QDs and $TiO_2$ nanorods (NiO nanosheets) were clearly observed, which provided more compelling evidence that QDs were remarkably attached onto the substrate surfaces (Figure S4). Furthermore, the estimated crystalline sizes of QDs through Scherrer's formula from XRD were approximately 6.5 and 5.0 nm for CdS and CdSe, which were consistent with the observation from HRTEM images. The significant QD decoration could be further revealed by the fact that well-resolved interplanar spacings of 0.325, 0.336, 0.241, and 0.348 nm correspond to the (110) plane of rutile $TiO_2$, the (002) plane of wurtzite CdS, the (111) plane of NiO, and the (111) plane of zinc blende CdSe, respectively. Figure 3a shows the absorption spectra of bare NiO nanosheets, $TiO_2$ nanorods, CdSe QD modified NiO nanosheets, and CdS QD modified $TiO_2$ nanorods. The inset in Figure 3a displays photographs of a CdSe QD modified NiO photocathode and a CdS QD modified $TiO_2$ photoanode. The absorption spectra of the CdSe QD modified NiO photocathode and CdS QD modified $TiO_2$ photoanode exhibited a significant increase in the visible region, owing to the presence of either CdS or CdSe QDs, implying that the use of CdS or CdSe QDs as sensitizer enables a wider range of visible photons in sunlight to be harvested. The CdS QD modified $TiO_2$ photoanode and CdSe QD modified NiO photocathode absorb in the visible region with an onset at ~500 nm and ~630 nm,

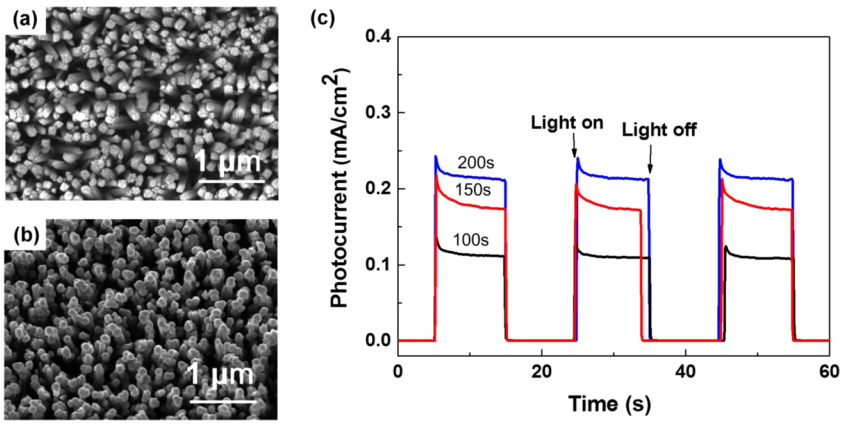


**Figure 5. (a) SEM image of bare $TiO_2$ nanorod array. (b) SEM image of CdS QD (200 s) coated $TiO_2$ nanorod array. (c) Transient photocurrent response curves of CdS-modified $TiO_2$ photoanode prepared with various electrodeposition times at 0 V *vs* Ag/AgCl.**

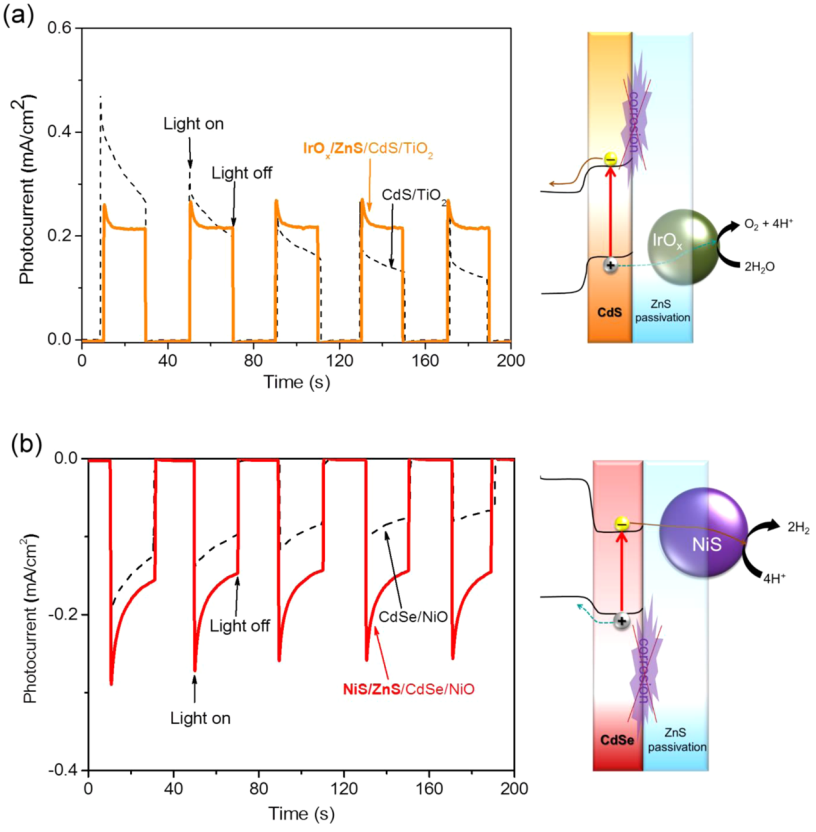


**Figure 6. (a) Photocurrent density *versus* time of ZnS coating and $IrO_x$ cocatalyst loading on a CdS/$TiO_2$ nanorod photoanode measured at 0 V *vs* Ag/AgCl. (b) Photocurrent density *versus* time of ZnS coating and NiS cocatalyst loading on a CdSe/NiO nanosheet photocathode measured at 0 V *vs* Ag/AgCl. Simulated 1 sun illumination (AM1.5G) with UV cutoff ($\lambda > 400$ nm) was used, and the scan rate is 10 mV/s.**

corresponding to the presence of CdS QDs and CdSe QDs, respectively, consistent with the observation in the absorption spectra (Figure 1c). To quantify the photoresponse of QD-sensitized photoelectrodes, incident-photon-to-current-conversion efficiency (IPCE) measurements were made to examine their photoresponses as a function of incident light wavelength (Figure 3b). IPCE can be expressed as[28,39,40]

$$\text{IPCE} = [1240 \times I(\lambda)]/[\lambda \times P(\lambda)]$$

where $I(\lambda)$ is the photocurrent, $P(\lambda)$ is the illumination power, and $\lambda$ is the wavelength of incident light. The photoresponses of $TiO_2$ and NiO photoelectrodes were drastically extended to the visible light region of the solar spectrum after modification of cadmium chalcogenide QDs, indicating that photogenerated charge carriers by excitation of cadmium chalcogenide QDs can efficiently inject into both $TiO_2$ and NiO and considerably contribute to photocurrent generation. Notably, a $TiO_2$ nanorod photoanode sensitized with CdS QDs exhibited a

substantially higher IPCE than a CdSe QD modified NiO photocathode, attributed primarily to their intrinsic n-type nature of cadmium chalcogenide QDs. In the case of the CdS QD modified $TiO_2$ photoanode, the band-bending effect within CdS QDs is able to facilitate the charge separation and advance charge transfer in the interface of the QDs and electrolyte. However, the n-type nature of CdSe QDs as a photocathode sensitizer might generate a negative effect on their charge transferring within the semiconductor surface and electrolyte interface. To eliminate this negative effect, co-modification of ZnS and gas evolution cocatalysts are consequently utilized in the following section. Overall, the IPCE of a CdS QD modified $TiO_2$ photoanode and a CdSe QD modified NiO photocathode revealed significant photoresponses in the visible light region, which is consistent with the observed increase in visible light absorption after CdS or CdSe QD modification.

Chemical bath deposition growth of CdSe QDs was optimized as well since decoration of QDs would strongly affect the photoelectrochemical performance of the CdSe/NiO photocathode. Figure 4a–d shows the SEM images of a CdSe QD modified NiO nanosheet photocathode with various CBD growth times. A CdSe QD single layer could be uniformly loaded on both sides of the NiO nanosheet if the deposition time was less than 24 h, which is beneficial for efficient charge carrier separation at the interface of the CdSe QDs/NiO nanosheet. However, in the case of longer CBD growth (more than 36 h), the formation of CdSe QD aggregations on the NiO nanosheets forced the charge carriers to diffuse longer distances, resulting in a greater recombination loss and thus poorer photoelectrochemical performance.[29,41] The best cathodic photocurrent at 0 V *vs* Ag/AgCl for the CdSe/NiO photocathode is ~0.13 mA/cm$^2$, in which the photoelectrode was prepared with 24 h CBD growth of CdSe (Figure 4e). On the other hand, CdS QDs were used to modify the $TiO_2$ nanorod photoanode to extend the optical response to visible light in this work, where CdS QDs were deposited onto a $TiO_2$ nanorod array by using a modified electrochemical deposition method.[42] The optimized CdS/$TiO_2$ photoanode delivers a photocurrent density of ~0.30 mA/cm$^2$ at 0 V *vs* Ag/AgCl under 1 sun visible light illumination (1 sun illumination with UV $\lambda < 400$ nm filtered off) (Figure 5).

**Passivation of Photoelectrodes.** Since cadmium chalcogenide QDs commonly suffer from photodecomposition and/or photocorrosion in aqueous media under illumination, a sacrificial reagent such as sulfide or selenium ions was generally employed to protect QDs from undesired photogenerated effects. However, sacrificial reagents normally contain reductant, electron donors, or hole scavengers; photogenerated charge carriers consequently react with sacrificial reagents rather than water, resulting in the fact that either a cathodic or anodic reaction can be performed

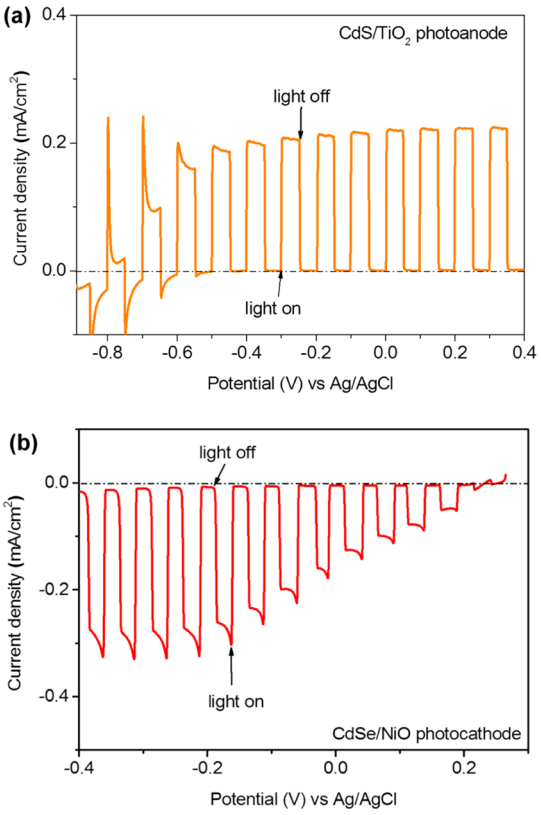


**Figure 7. *J*–*V* scans of CdS QD modified $TiO_2$ nanorod photoanode (a) and CdSe QD modified NiO nanosheet photocathode (b) under chopped illumination (all samples were co-modified with ZnS and gas evolution cocatalysts).**

under a sacrificial environment. As a result, a sacrificial system cannot be operated to protect QDs for solar water splitting. Although optimized decoration of QDs can facilitate effective charge transferring to improve their stability,[27] this still cannot offer sufficient stability for long-term irradiation. Consequently, an easily synthesized corrosion-resistant layer that can protect the underlying semiconductor QDs while not inhibiting charge carrier (electron or hole) transport and photon absorption will be extremely essential. In the present study, a thin protecting layer of ZnS and NiS or iridium oxide nanoparticles as hydrogen or oxygen evolution cocatalysts was sequentially decorated on the surfaces of CdSe/NiO and CdS/$TiO_2$ photoelectrodes. Iridium oxide and NiS have been demonstrated to significantly catalyze oxygen evolution and hydrogen evolution reactions,[43–45] which allow us to improve their activities in both the photoanode and photocathode (Figure S5). The ZnS layer has been reported to act as a passivation layer to protect QDs and increase photocurrent in solar cells, where the ZnS layer can prevent the recombination of photogenerated electrons with oxidizers on the surface of QDs.[46,47] It has to be pointed out here that the stabilizing treatment of photoelectrodes in solar water splitting has to be different from solar cells, and both a ZnS overlayer and cocatalyst decoration are essential and critical for stabilizing

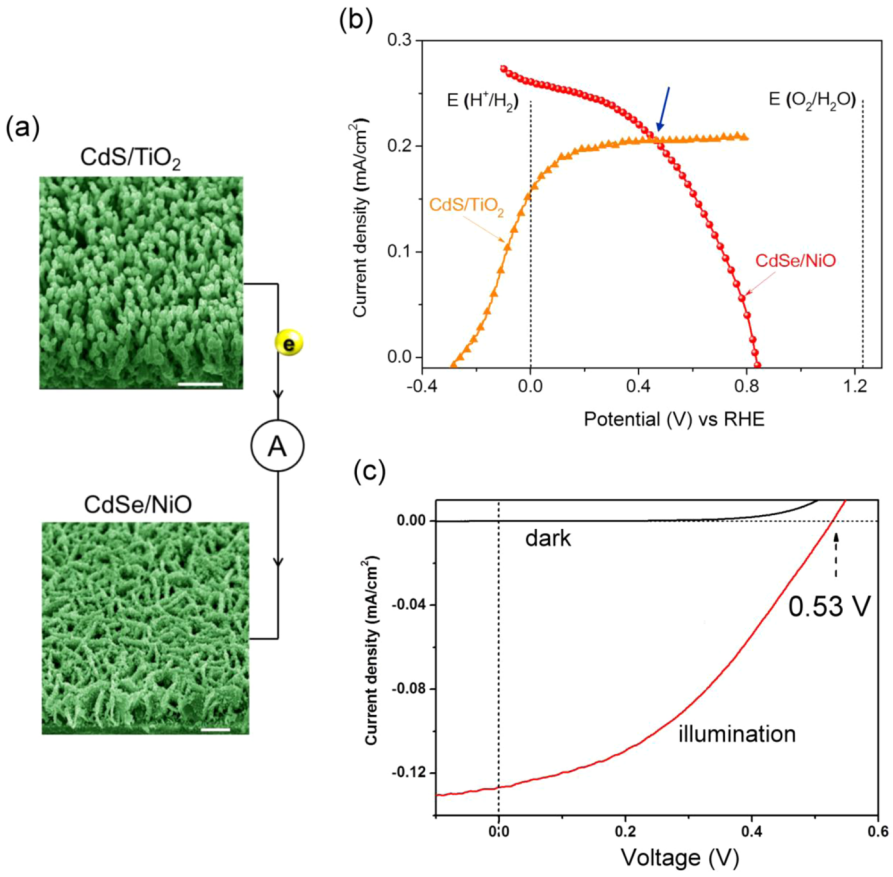


**Figure 8. (a) SEM images of CdS QD modified $TiO_2$ nanorod (top) and CdSe QD modified NiO nanosheet (bottom) electrodes. Scale bar: 500 nm. (b) Photocurrent density of CdS QD modified $TiO_2$ nanorod photoanode and CdSe QD modified NiO nanosheet photocathode in 0.5 M $Na_2SO_4$ solution *versus* the applied voltage referenced to a reversible hydrogen electrode (RHE). (c) *J*−*V* curve of a photoelectrolysis cell with CdS QD modified $TiO_2$ nanorod and CdSe QD modified NiO nanosheet photoelectrodes.**

cadmium chalcogenide QDs in solar water splitting systems, in which ZnS passivation and cocatalysts are responsible for QD protection and charge carrier extraction, respectively (as shown in Figure 6). This co-modification of the ZnS layer and gas evolution co-catalysts can perform a nearly identical photoresponse within the measured period in both the photoanode and photocathode. By contrast, the QD-modified photoanode and photocathode without ZnS and co-catalyst decoration exhibited a substantial and rapid decrease in photocurrent, which verified that bare cadmium chalcogenide QD modified photoelectrodes are unable to achieve practical solar water splitting, as shown in Figure 6a and b. In the solar water splitting system, ZnS passivation alone cannot provide sufficient efforts for enhancing performance since both anodic and cathodic reactions need to be simultaneously considered. If only a ZnS layer is employed to passivate QDs from surface recombination, further increasing the thickness of the passivation layer will result in a negative effect and lead to a decrease in photocurrent (not shown here), since a thicker ZnS layer simultaneously suppresses both anodic and cathodic reactions to reduce the overall performance of water splitting. For example, ZnS passivation can suppress the recombination at surface trapping states on CdS QDs and facilitate the electron flow from CdS to $TiO_2$, but anodic reaction (water oxidation for oxygen evolution) would be simultaneously passivated as well. Toward this end, cocatalysts (iridium oxide) are essentially utilized to facilitate the collection of holes and to improve oxygen evolution in water splitting. Effectively collecting charge carriers can not only improve the photocurrent but also avoids the undesired photogenerated effect on QDs. Co-modification of ZnS and gas evolution cocatalysts are greatly able to suppress surface state trapping to enhance photocurrent and efficiently collect carriers to improve gas evolution in a solar water splitting system. As a result, the optimized photocurrent−photovoltage (*J*−*V*) data under chopped illumination are plotted in Figure 7a and b. The onset potential and saturation photocurrent for the CdS/$TiO_2$ photoanode were found to be −0.83 V *vs* Ag/AgCl and 0.21 mA/$cm^2$, respectively. The CdSe/NiO photocathode gave a cathodic photocurrent with an onset potential at 0.23 V *vs* Ag/AgCl and a photocurrent density of 0.30 mA/$cm^2$ at −0.4 V *vs* Ag/AgCl.

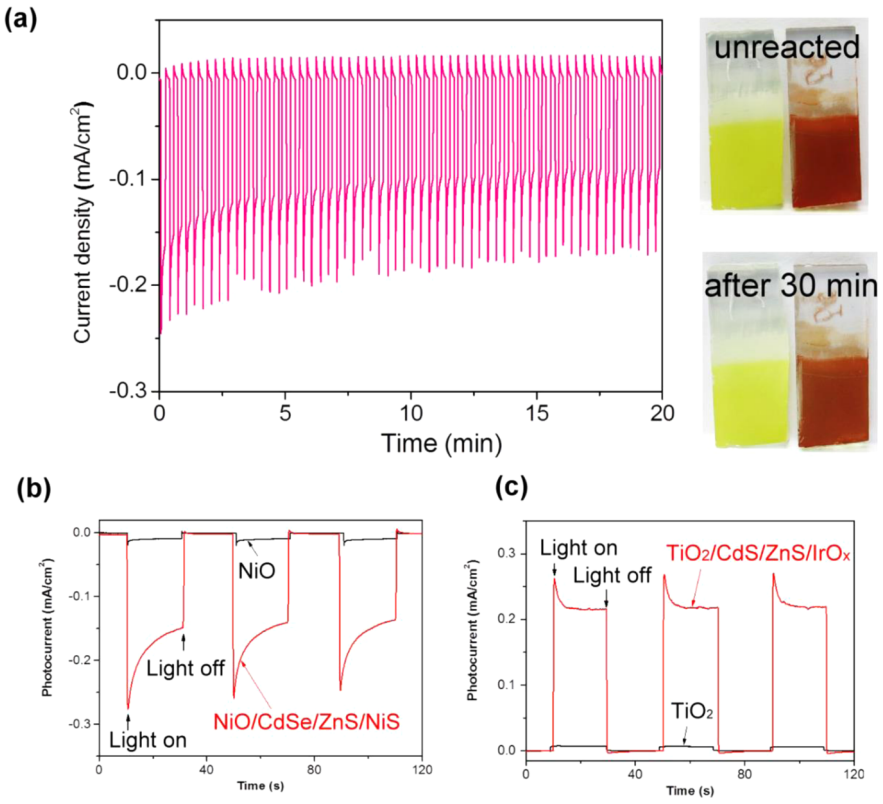


**Figure 9. (a) Photocurrent density *versus* time of externally short-circuited CdS QD modified $TiO_2$ nanorod and CdSe QD modified NiO nanosheet photoelectrodes under chopped light exposure. Inset: Digital photographs of CdS/$TiO_2$ photoanode and CdSe/NiO photocathode before and after 30 min of continuous photoreaction. Photocurrent responses of (b) bare $TiO_2$ nanorod array and optimized CdS/$TiO_2$ nanorod photoanode and (c) bare NiO nanosheet array and optimized CdSe/NiO nanosheet photocathode at 0 V *vs* Ag/AgCl.**

**Wire-Linked Photoelectrodes.** To further reveal solar-driven water splitting, a wire-linked photoelectrolysis cell was obtained (as shown in Figure 8a), in which the optimized individual $J-V$ curve for the CdSe/NiO photocathode and CdS/$TiO_2$ photoanode under simulated sunlight with UV filtered-off was measured (Figure 8b). In this individual measurement, a current density intersection of 0.19 mA/cm$^2$ (as indicated by the arrow) suggests a nonzero current flow under visible light illumination once the CdSe/NiO photocathode and CdS/$TiO_2$ photoanode are directly linked. Further measuring the $J-V$ curve of the wire-linked photoelectrolysis cell in a tandem configuration demonstrated the open-circuit voltage ($V_{oc}$) of the photoelectrolysis cell is ~0.53 V (Figure 8c and Figure S6), which can be attributed to the sum of photovoltages of the CdS/$TiO_2$ photoanode (~−0.42 V) and CdSe/NiO photocathode (~0.13 V) (Figure S7). This phenomenon is clearly consistent with the observation in Figure 8b, implying that overall solar-driven water splitting can be spontaneously performed without applied external energy in a tandem configuration of CdSe/NiO and CdS/$TiO_2$ photoelectrodes. A short-circuit current density of ~0.125 mA/cm$^2$ is obtained under 1 sun visible light illumination, which is further confirmed through corresponding transient photocurrent response of this tandem cell under chopped visible light illumination (Figure S8).

Prolonged testing of the two illuminated cadmium chalcogenide QD modified photoelectrodes under short-circuit conditions was also performed; a photocurrent *versus* time evolution of the photoelectrolysis system under chopped illumination over 20 min is shown in Figure 9a. The photocurrent first decreased and then stabilized at ~70% of its original performance, rendering a stabilized photocurrent density of 0.11 mA/cm$^2$ under simulated 1 sun illumination with UV filtered-off, indicating that this co-modification can significantly stabilize the cadmium chalcogenide QDs under long irradiation. Furthermore, no obvious change in appearance of the QD-modified photoelectrodes after 30 min of continuous photoreaction was observed (inset), indicating that this co-modification of ZnS and gas evolution cocatalysts can significantly improve their properties in both surface passivation of QDs and charge-carrier transferring between QDs/$TiO_2$(NiO) and exhibit a good system photostability (Figure S9). In addition, the photocurrent contributions from bare NiO and $TiO_2$ photoelectrodes are merely 9 and 7 $\mu$A/cm$^2$ (Figure 9b and c); this finding revealed that wide-band-gap materials ($TiO_2$ and NiO) generated an extremely low photoresponse (~4% and ~5%)

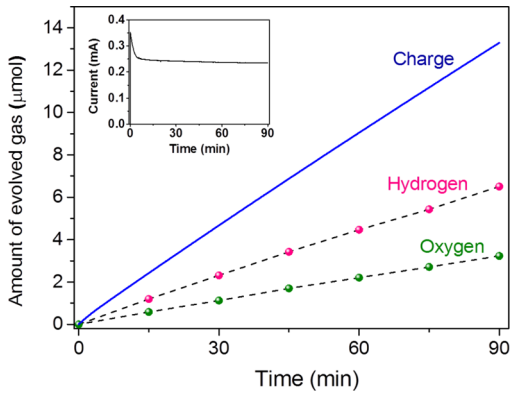


**Figure 10. Comparison of the evolved hydrogen and oxygen gases and the charge through the external circuit. Inset in e shows the photocurrent *versus* time measurement.**

compared to that of a QD-modified photocathode and photoanode, indicating that the photoresponse from $TiO_2$ or NiO is negligible and all photocurrent results from the photogenerating process of cadmium chalcogenide QDs in the visible light region. Consequently, a visible-light-driven spontaneous water splitting has been realized, while the calculated overall solar-to-chemical conversion efficiency based on photocurrent density is ~0.17%, which is comparable to the efficiency of natural photosynthesis.[2,20]

Figure 10 displays the evolution of $H_2$ and $O_2$ gases in a 0.5 M $Na_2SO_4$ aqueous solution. A stoichiometric amount of $H_2$ and $O_2$ with a hydrogen-to-oxygen ratio of 2:1 was observed, which is expected as a result of spontaneous water splitting. Moreover, the amount of $H_2$ evolved is almost equal to half of the charges that passed through the external circuit, giving a high charge-to-chemical faradic efficiency of ~95%.

## CONCLUSIONS

In summary, a photoelectrolysis cell with a cadmium chalcogenide QD modified $TiO_2$ nanorod photoanode and a NiO nanosheet photocathode was developed for spontaneous overall water splitting to produce $H_2$ and $O_2$ under visible light illumination. Such a self-driven water splitting system provides desired charge transfer paths to achieve high-efficiency $H_2$ and $O_2$ generation at zero external bias condition. The optimized CdSe QD modified NiO photocathode combined with a current-matched CdS QD modified $TiO_2$ photoanode gave rise to the highest efficiency of overall solar water splitting, about 0.17%. Average gas evolution rates of 2.24 (hydrogen) and 1.07 (oxygen) $\mu$mol $h^{-1}$ $cm^{-2}$ at zero bias condition have been achieved, with almost 95% faradic efficiency. In addition, this research provides a new concept of co-modification of the passivation layer and cocatalysts to suppress surface-state trapping and to efficiently collect charge carriers for enhancing overall efficiency of solar water splitting. Although this maiden concept focuses on cadmium chalcogenide quantum dots and $TiO_2$/NiO photoelectrodes, we believe that our strategy is fundamental to the design of solar energy devices and should become an accepted technique for solar energy utilization in spontaneous solar water splitting systems under visible light illumination.

## METHODS

**Materials.** Titanium isopropoxide, hydrochloric acid, cadmium chloride, sodium sulfide, sodium sulfate, sodium thiosulfate, zinc nitrate, nickel acetate, nickel nitrate, potassium persulfate, 3-mercaptopropionic acid (≥99%, Aldrich), nitrilotriacetic acid, sodium hydroxide, and aqueous ammonia were used as received without any further purification.

**CdS/$TiO_2$ Photoanode Preparation.** *Growth of $TiO_2$ Nanorod Array.* $TiO_2$ nanorod arrays were grown on fluorine-doped tin oxide substrate using a hydrothermal method. In a typical synthesis, FTO substrate (Tec 15, 10 Ω/□, Hartford Glass Company) was first cleaned with 5 wt % detergent in an ultrasonic water bath for 30 min, followed by rinsing with DI water and sonicating for another 10 min. After being dried by a $N_2$ stream, the FTO substrate was placed in a sealed Teflon-lined autoclave (63 mL), containing 20 mL of HCl (37 wt %), 20 mL of DI water, and 0.5 g of titanium isopropoxide. The hydrothermal reaction was conducted at 200 °C for 4 h. After the reaction, the $TiO_2$ nanorod covered FTO substrate was rinsed with DI water, dried at 70 °C, calcined at a ramp of 1 °C/min to 500 °C, and kept at this temperature for 1 h before loading CdS quantum dots.

*Electrochemical Deposition of CdS QDs.* CdS QDs were electrochemically deposited onto $TiO_2$ nanorod arrays from a solution containing 0.2 M $CdCl_2$ and 0.05 M $Na_2S_2O_3$. The pH of the solution was adjusted to 2.1 by adding a few drops of 0.1 M HCl. The electrochemical deposition was conducted at 70 °C using a three-electrode setup, with $TiO_2$/FTO as the working electrode, Pt plate as the counter electrode, and a standard calomel electrode (SCE) as the reference electrode. During deposition, a constant voltage of −0.7 V *vs* SCE was applied to the $TiO_2$/FTO working electrode for different times to optimize the coverage of CdS QDs on $TiO_2$ nanorod arrays.

*Coating of ZnS Protective Layer.* A thin ZnS protective layer was coated on the as-prepared CdS/$TiO_2$ photoelectrode using a successive ionic layer adsorption and reaction (SILAR) technique to improve the photostability. CdS/$TiO_2$ films were sequentially dipped into four different solutions of 0.05 M $Zn(NO_3)_2$, DI water, 0.05 M $Na_2S$, and DI water, respectively. The thickness of the ZnS protective layer was controlled by the number of dipping cycles.

**CdSe/NiO Photocathode Preparation.** *Growth of NiO Nanosheet Array.* NiO nanosheet arrays were grown on an FTO substrate using a chemical bath deposition technique. Prior to CBD growth, a compact NiO layer was deposited on the FTO substrate by spin-coating a nickel acetate (98%, Aldrich) ethanolic solution (0.4 M) on FTO at 2000 rpm and sintering at 350 °C for 30 min. Thermal annealing converts nickel acetate to nickel oxide through $Ni(CH_3COO)_2 + 4O_2 \rightarrow NiO + 4CO_2 + 3H_2O$. A solution for CBD growth of NiO nanosheets was prepared by mixing 80 mL of 1 M nickel nitrate, 60 mL of 0.25 M potassium persulfate, and 20 mL of aqueous ammonia (25−28%) in a 250 mL Pyrex beaker at room temperature. The NiO compact layer covered FTO substrates were placed vertically in the freshly prepared solution and kept at room temperature for 20 min to grow a NiOOH nanosheet precursor film. Then, the NiOOH nanosheet film was dried at 70 °C, heated at a ramp of 1 °C/min to 450 °C, and kept at this temperature for 1 h to convert NiOOH to NiO.

*CBD Growth of CdSe Nanoparticles.* CdSe nanoparticles were coated on NiO nanosheet arrays using a CBD technique. Prior to CBD growth of CdSe nanoparticles, the NiO nanosheet film was immersed in 10 mM 3-mercaptopropionic acid (MPA) solution for 1 h at 40 °C under a nitrogen atmosphere to anchor a monolayer of MPA molecules onto NiO through −COO−NiO binding. The films were then transferred into a 25 mM $CdCl_2$ aqueous solution for 1 h at 40 °C under a nitrogen atmosphere to adsorb $Cd^{2+}$ ions on the surface of the NiO nanosheets, which serve as nucleation centers for CdSe nanoparticle growth. The CBD growth solution was prepared by mixing 10 mL of 80 mM $CdCl_2$ and 10 mL of 80 mM sodium selenosulfate ($Na_2SeSO_3$) solution with 10 mL of 120 mM trisodium nitrilotriacetate [$N(CH_2COONa)_3$]. The CBD growth was conducted at 10 °C for different times to grow CdSe nanoparticles with different CdSe coverage.

**Preparation and Loading of Hydrogen Evolution Reaction (HER) and Oxygen Evolution Reaction (OER) Cocatalysts.** *HER Cocatalyst.* NiS nanoparticles were used as the cocatalysts for the hydrogen evolution reaction. Loading of NiS nanoparticles onto a CdSe/NiO photocathode was performed using the SILAR technique by alternatively dipping the photocathode into 0.05 M $Ni(NO_3)_2$ and 0.05 M $Na_2S$ ethanolic solutions for 2 min per dip and subsequently rinsing with ethanol. Afterward, the electrode was washed a few times with deionized water and blow-dried with nitrogen.

*OER Cocatalyst.* $IrO_x \cdot nH_2O$ nanoparticles were used as the cocatalysts for the oxygen evolution reaction. The colloidal $IrO_x \cdot nH_2O$ suspension was prepared by hydrolysis of a 2 mM $K_2IrCl_6$ aqueous solution at pH = 13. The hydrolysis was carried out at 90 °C for 20 min. Then, the pH of the solution was rapidly adjusted to 1 by adding a 3 M $HNO_3$ aqueous solution in an ice bath and maintained for 80 min to induce acid condensation. After adjusting the suspension pH to 7, the ZnS-protected $CdS/TiO_2$ nanorod array was immersed into the $IrO_x \cdot nH_2O$ colloidal suspension for 1 h to adsorb $IrO_x \cdot nH_2O$ nanoparticles onto the electrode. Afterward, the electrode was washed a few times with deionized water and blow-dried with nitrogen.

**Characterization.** The crystal structure and morphology of cadmium chalcogenide QD modified photoelectrodes were examined with X-ray diffraction (Bruker AXS D8 Advance), field-emission scanning electron microscopy (JEOL JSM-6700F), and transmission electron microscopy (TEM, JEOL JEM-2100F), respectively. Absorption spectra were recorded using a PerkinElmer Lambda 900 UV−vis−NIR spectrometer equipped with an integrating sphere. Photoluminescence spectra and photoluminescence lifetime spectroscopy were measured at room temperature using a commercial laser-flash photolysis spectrometer (Edinburgh Instruments LP920-KS), a photomultiplier tube (Hamamatsu R928), a gated CCD (Princeton Instruments, PI-MAX ICCD camera), and a digital oscilloscope (Tektronix TDS-3012C). The sample was prepared by attaching a calculated amount of CdS or CdSe QDs synthesized from a hot injection method onto $TiO_2$ nanorods or NiO nanosheets and excited using a 420 nm laser pulse (5 ns duration, ~2 mJ $cm^{-2}$). Detailed chemical composition of samples was obtained by X-ray photoelectron spectroscopy (XPS) measurements on an ESCALAB 250 photoelectron spectrometer (Thermo Fisher Scientific) at $2.4 \times 10^{-10}$ mbar using a monochromatic Al Kα X-ray beam (1486.60 eV). All binding energies were referenced to the C 1s peak (284.60 eV) arising from adventitious hydrocarbons.

**Photoelectrochemical Measurements.** Photoelectrochemical properties of individual cadmium chalcogenide QD modified photoanode and photocathode were measured using an electrochemical workstation (WonA tech, ZIVE SP2) in a standard three-electrode setup with a Pt plate as the counter electrode and Ag/AgCl as the reference electrode. Reproducibility of all measurements was precisely controlled within 10% for different batch samples to achieve significant comparisons. The short-circuit measurements of the externally wired $CdS/TiO_2$ nanorod photoanode and CdSe/NiO nanosheet photocathode were performed using a two-electrode setup, in which the electrochemical workstation remained short-circuited and behaved as an ammeter. The two photoelectrodes were in the same reactor and placed in a tandem configuration ($CdS/TiO_2$ photoanode as front cell and CdSe/NiO photocathode as back cell), as illustrated in Figure 1. In all cases, a 0.5 M $Na_2SO_4$ aqueous solution (pH = 6.8) was used as the electrolyte. The light source used for simulated sunlight was a 300 W xenon lamp (Newport, Oriel, 91160) equipped with an AM1.5G filter (Newport, 81094) and a UV filter (Newport, FSQ-GG400) (>400 nm). Prior to each measurement, the light intensity was determined by a calibrated silicon photodiode. The incident photon-to-current conversion efficiency was measured under zero-bias (two-electrode, short-circuit) condition. The monochromatic light was supplied by a xenon lamp (450 W, Oriel) illuminating through a monochromator (Newport) with a bandwidth of 5 nm. The photoactivity of the two short-circuited photoelectrodes was characterized by measuring the gaseous products using a commercial compact glass photoreactor system (Makuhari Rikagaku Garasu Inc. CCS-N-66-76). The setup comprises a quartz batch reactor, a circulation system, a vacuum pump, and a gas chromatograph (Agilent 490 Micro GC) for inline measurements.

**Calculation of the Energy Conversion Efficiency and Faradic Efficiency.** The energy conversion efficiency of the solar-driven water splitting ($\eta$) was calculated based on the measured photocurrent density, using the following equation:

$$\eta = \frac{1.23(\mathrm{V}) \times I(\mathrm{mA/cm^2})}{P(\mathrm{mW/cm^2})} \times 100\%$$

in which $I$ is the photocurrent density and $P$ is the light intensity. For the calculation of the faradic efficiency of the water splitting ($\eta_{\mathrm{faradic}}$) in the configuration of short-circuited electrodes, the following equation was applied:

$$\eta_{\mathrm{faradic}} = \frac{2 \times n_{\mathrm{H_2}}(\mathrm{mol}) \times 96485(\mathrm{C/mol})}{Q(\mathrm{C})} \times 100\%$$

in which $Q$ is the total amount of charge passed through the external circuit during the same time period as the measurement of evolved $H_2$ gas.

*Conflict of Interest:* The authors declare no competing financial interest.

*Supporting Information Available:* SEM images of FTO and NiO compact layer coated FTO. Photocurrent *versus* time plot of a CdSe/NiO photoelectrode without a NiO compact layer at zero bias condition. High-magnification SEM and TEM images of $CdS/TiO_2$ and CdSe/NiO photoelectrodes. IPCE spectra at different applied external biases. XPS spectra of protective layer and cocatalyst-modified photoelectrodes. $J-V$ curves of photoelectrolysis cell. The effect of oxygen-generating $IrO_x \cdot nH_2O$ nanoparticles on a $ZnS/CdS/TiO_2$ nanorod photoanode and the hydrogen-generating NiS nanoparticles on a ZnS/CdSe/NiO nanosheet photocathode. Photovoltage *versus* time curves of the NiO photocathode and $TiO_2$ under visible light. Transient photocurrent response curve of the wire-linked photoanode and photocathode system. This material is available free of charge *via* the Internet at http://pubs.acs.org.

*Acknowledgment.* The authors acknowledge Nanyang Technological University, the Singapore-Berkeley Research Initiative for Sustainable Energy (SinBeRISE), and the Ministry of Science and Technology in Taiwan (Contract No. NSC 102-2113-M-002-013-MY2) for financial support. We thank Prof. Chen Wei from the Department of Chemistry at National University of Singapore for help with XPS measurement.

## REFERENCES AND NOTES

1. Gray, H. B. Powering the Planet with Solar Fuel. *Nat. Chem.* **2009**, *1*, 7–7.
2. Blankenship, R. E.; Tiede, D. M.; Barber, J.; Brudvig, G. W.; Fleming, G.; Ghirardi, M.; Gunner, M. R.; Junge, W.; Kramer, D. M.; Melis, A.; *et al.* Comparing Photosynthetic and Photovoltaic Efficiencies and Recognizing the Potential for Improvement. *Science* **2011**, *332*, 805–809.
3. Graydon, O. Solar Cells: Benefit of Strain. *Nat. Photonics* **2011**, *5*, 712–712.
4. Sargent, E. H. Colloidal Quantum Dot Solar Cells. *Nat. Photonics* **2012**, *6*, 133–135.

5. Tachibana, Y.; Vayssieres, L.; Durrant, J. R. Artificial Photosynthesis for Solar Water-Splitting. *Nat. Photonics* **2012**, *6*, 511–518.
6. Anscombe, N. Solar Cells that Mimic Plants. *Nat. Photonics* **2011**, *5*, 266–267.
7. Meyer, T. J. Catalysis - The Art of Splitting Water. *Nature* **2008**, *451*, 778–779.
8. Fujishima, A.; Honda, K. Electrochemical Photolysis of Water at a Semiconductor Electrode. *Nature* **1972**, *238*, 37–38.
9. Warren, S. C.; Voitchovsky, K.; Dotan, H.; Leroy, C. M.; Cornuz, M.; Stellacci, F.; Hebert, C.; Rothschild, A.; Graetzel, M. Identifying Champion Nanostructures for Solar Water-Splitting. *Nat. Mater.* **2013**, *12*, 842–849.
10. Brillet, J.; Yum, J.-H.; Cornuz, M.; Hisatomi, T.; Solarska, R.; Augustynski, J.; Graetzel, M.; Sivula, K. Highly Efficient Water Splitting by a Dual-Absorber Tandem Cell. *Nat. Photonics* **2012**, *6*, 823–827.
11. Maeda, K.; Takata, T.; Hara, M.; Saito, N.; Inoue, Y.; Kobayashi, H.; Domen, K. GaN: ZnO Solid Solution as a Photocatalyst for Visible-Light-Driven Overall Water Splitting. *J. Am. Chem. Soc.* **2005**, *127*, 8286–8287.
12. Maeda, K.; Teramura, K.; Lu, D. L.; Takata, T.; Saito, N.; Inoue, Y.; Domen, K. Photocatalyst Releasing Hydrogen from Water- Enhancing Catalytic Performance Holds Promise for Hydrogen Production by Water Splitting in Sunlight. *Nature* **2006**, *440*, 295–295.
13. Kudo, A.; Miseki, Y. Heterogeneous Photocatalyst Materials for Water Splitting. *Chem. Soc. Rev.* **2009**, *38*, 253–278.
14. Nozik, A. J. P-N Photoelectrolysis Cells. *Appl. Phys. Lett.* **1976**, *29*, 150–153.
15. Walter, M. G.; Warren, E. L.; McKone, J. R.; Boettcher, S. W.; Mi, Q. X.; Santori, E. A.; Lewis, N. S. Solar Water Splitting Cells. *Chem. Rev.* **2010**, *110*, 6446–6473.
16. Gratzel, M. Photoelectrochemical Cells. *Nature* **2001**, *414*, 338–344.
17. Bolton, J. R.; Strickler, S. J.; Connolly, J. S. Limiting and Realizable Efficiencies of Solar Photolysis of Water. *Nature* **1985**, *316*, 495–500.
18. Faunce, T.; Styring, S.; Wasielewski, M. R.; Brudvig, G. W.; Rutherford, A. W.; Messinger, J.; Lee, A. F.; Hill, C. L.; deGroot, H.; Fontecave, M.; *et al*. Artificial Photosynthesis as a Frontier Technology for Energy Sustainability. *Energy Environ. Sci.* **2013**, *6*, 1074–1076.
19. McConnell, I.; Li, G.; Brudvig, G. W. Energy Conversion in Natural and Artificial Photosynthesis. *Chem. Biol.* **2010**, *17*, 434–447.
20. Barber, J. Photosynthetic Energy Conversion: Natural and Artificial. *Chem. Soc. Rev.* **2009**, *38*, 185–196.
21. Nocera, D. G. The Artificial Leaf. *Acc. Chem. Res.* **2012**, *45*, 767–776.
22. Nozik, A. J. Photochemical Diodes. *Appl. Phys. Lett.* **1977**, *30*, 567–569.
23. Ohashi, K.; Mccann, J.; Bockris, J. O. M. Stable Photoelectrochemical Cells for Splitting of Water. *Nature* **1977**, *266*, 610–611.
24. Liu, C.; Tang, J. Y.; Chen, H. M.; Liu, B.; Yang, P. A Fully Integrated Nanosystem of Semiconductor Nanowires for Direct Solar Water Splitting. *Nano Lett.* **2013**, *13*, 2989–2992.
25. Chen, H. M.; Chen, C. K.; Liu, R.-S.; Zhang, L.; Zhang, J.; Wilkinson, D. P. Nano-architecture and Material Designs for Water Splitting Photoelectrodes. *Chem. Soc. Rev.* **2012**, *41*, 5654–5671.
26. Kamat, P. V. Quantum Dot Solar Cells. The Next Big Thing in Photovoltaics. *J. Phys. Chem. Lett.* **2013**, *4*, 908–918.
27. Chen, H. M.; Chen, C. K.; Chang, Y. C.; Tsai, C. W.; Liu, R. S.; Hu, S. F.; Chang, W. S.; Chen, K. H. Quantum Dot Monolayer Sensitized ZnO Nanowire-Array Photoelectrodes: True Efficiency for Water Splitting. *Angew. Chem., Int. Ed.* **2010**, *49*, 5966–5969.
28. Wang, G. M.; Yang, X. Y.; Qian, F.; Zhang, J. Z.; Li, Y. Double-Sided CdS and CdSe Quantum Dot Co-Sensitized ZnO Nanowire Arrays for Photoelectrochemical Hydrogen Generation. *Nano Lett.* **2010**, *10*, 1088–1092.
29. Miao, J.; Yang, H.; Khoo, S. Y.; Liu, B. Electrochemical Fabrication of ZnO/CdSe Core-Shell Nanorod Arrays for Efficient Photoelectrochemical Water Splitting. *Nanoscale* **2013**, *5*, 11118.
30. Xiao, F.-X.; Miao, J.; Liu, B. Layer-by-Layer Self-Assembly of CdS Quantum Dots/Graphene Nanosheets Hybrid Films for Photoelectrochemical and Photocatalytic Applications. *J. Am. Chem. Soc.* **2014**, *136*, 1559–1569.
31. Xiao, F.-X.; Miao, J.; Wang, H.-Y.; Liu, B. Self-Assembly of Hierarchically Ordered CdS Quantum Dots-$TiO_2$ Nanotube Array Heterostructures as Efficient Visible Light Photocatalysts for Photoredox Applications. *J. Mater. Chem. A* **2013**, *1*, 12229–12238.
32. Irwin, M. D.; Buchholz, B.; Hains, A. W.; Chang, R. P. H.; Marks, T. J. p-Type Semiconducting Nickel Oxide as an Efficiency-Enhancing Anode Interfacial Layer in Polymer Bulk-Heterojunction Solar Cells. *P. Natl. Acad. Sci. U.S.A.* **2008**, *105*, 2783–2787.
33. Nattestad, A.; Mozer, A. J.; Fischer, M. K. R.; Cheng, Y. B.; Mishra, A.; Baeuerle, P.; Bach, U. Highly Efficient Photocathodes for Dye-Sensitized Tandem Solar Cells. *Nat. Mater.* **2010**, *9*, 31–35.
34. Nakaoka, K.; Ueyama, J.; Ogura, K. Semiconductor and Electrochromic Properties of Electrochemically Deposited Nickel Oxide Films. *J. Electroanal. Chem.* **2004**, *571*, 93–99.
35. Chan, I. M.; Hsu, T. Y.; Hong, F. C. Enhanced Hole Injections in Organic Light-Emitting Devices by Depositing Nickel Oxide on Indium Tin Oxide Anode. *Appl. Phys. Lett.* **2002**, *81*, 1899–1901.
36. Kang, S. H.; Zhu, K.; Neale, N. R.; Frank, A. J. Hole Transport in Sensitized CdS-NiO Nanoparticle Photocathodes. *Chem. Commun.* **2011**, *47*, 10419–10421.
37. Xia, X. H.; Tu, J. P.; Zhang, J.; Wang, X. L.; Zhang, W. K.; Huang, H. Electrochromic Properties of Porous NiO Thin Films Prepared by a Chemical Bath Deposition. *Sol. Energy Mater. Sol. C* **2008**, *92*, 628–633.
38. Rodenas, P.; Song, T.; Sudhagar, P.; Marzari, G.; Han, H.; Badia-Bou, L.; Gimenez, S.; Fabregat-Santiago, F.; Mora-Sero, I.; Bisquert, J.; *et al*. Quantum Dot Based Heterostructures for Unassisted Photoelectrochemical Hydrogen Generation. *Adv. Energy Mater.* **2013**, *3*, 176–182.
39. Park, J. H.; Kim, S.; Bard, A. J. Novel Carbon-Doped $TiO_2$ Nanotube Arrays with High Aspect Ratios for Efficient Solar Water Splitting. *Nano Lett.* **2006**, *6*, 24–28.
40. Yang, X.; Wolcottt, A.; Wang, G.; Sobo, A.; Fitzmorris, R. C.; Qian, F.; Zhang, J. Z.; Li, Y. Nitrogen-Doped ZnO Nanowire Arrays for Photoelectrochemical Water Splitting. *Nano Lett.* **2009**, *9*, 2331–2336.
41. Lightcap, I. V.; Kamat, P. V. Fortification of CdSe Quantum Dots with Graphene Oxide. Excited State Interactions and Light Energy Conversion. *J. Am. Chem. Soc.* **2012**, *134*, 7109–7116.
42. Banerjee, S.; Mohapatra, S. K.; Das, P. P.; Misra, M. Synthesis of Coupled Semiconductor by Filling 1D $TiO_2$ Nanotubes with CdS. *Chem. Mater.* **2008**, *20*, 6784–6791.
43. Gambardella, A. A.; Feldberg, S. W.; Murray, R. W. Electron Transfer Dynamics of Iridium Oxide Nanoparticles Attached to Electrodes by Self-Assembled Monolayers. *J. Am. Chem. Soc.* **2012**, *134*, 5774–5777.
44. Zhao, Y.; Hernandez-Pagan, E. A.; Vargas-Barbosa, N. M.; Dysart, J. L.; Mallouk, T. E. A High Yield Synthesis of Ligand-Free Iridium Oxide Nanoparticles with High Electrocatalytic Activity. *J. Phys. Chem. Lett.* **2011**, *2*, 402–406.
45. Zhang, W.; Wang, Y.; Wang, Z.; Zhong, Z.; Xu, R. Highly Efficient and Noble Metal-Free NiS/CdS Photocatalysts for $H_2$ Evolution from Lactic Acid Sacrificial Solution under Visible Light. *Chem. Commun.* **2010**, *46*, 7631–7633.
46. Santra, P. K.; Kamat, P. V. Mn-Doped Quantum Dot Sensitized Solar Cells: A Strategy to Boost Efficiency over 5%. *J. Am. Chem. Soc.* **2012**, *134*, 2508–2511.
47. Lee, Y.-L.; Chi, C.-F.; Liau, S.-Y. CdS/CdSe Co-Sensitized $TiO_2$ Photoelectrode for Efficient Hydrogen Generation in a Photoelectrochemical Cell. *Chem. Mater.* **2010**, *22*, 922–927.